ADVANCED QUANTUM TECHNOLOGIES
www.advquantumtech.com

A Tolerance-Enhanced Spontaneous Parametric Downconversion Source of Bright Entangled Photons

Sandeep Singh, Vimlesh Kumar, Anirban Ghosh, Andrew Forbes, and G. K. Samanta*

Spontaneous parametric down-conversion (SPDC), a primary resource of photonic quantum entangled states, strongly depends on the intrinsic phase matching condition. This makes it susceptible to changes in factors such as the pump wavelength, crystal temperature, and crystal axes orientation. Such intolerance to changing environmental factors prohibits deployment of SPDC-based sources in non-ideal environments outside controlled laboratories. Here, a novel system architecture based on a hybrid linear and non-linear solution that is shown to make the source tolerance-enhanced without sacrificing brightness. This linear solution is a lens-axicon pair, judiciously placed, which is tested together with two common non-linear crystals, quasi-phase-matched periodically-poled $KTiOPO_4$, and birefringent-phase-matched BiB_3O_6. This approach has the benefit of simultaneous tolerance to the environment and high brightness, which is demonstrated by using the proposed architecture as a stable entangled photon source and a spectral brightness as high as 22.58 ± 0.15 kHz mW^{-1} with a state fidelity of 0.95 ± 0.02, yet requiring a crystal temperature stability of only ±0.8 °C, a 5× enhanced tolerance as compared to the conventional high brightness SPDC configurations is reported. This solution offers a new approach to deployable high-brightness quantum sources that are robust to their environment, for instance, in satellite-based quantum applications.

1. Introduction

The most prominent manifestation of non-locality proposed by quantum mechanics, commonly known as quantum entanglement,[1] has found its implications in various domains, including quantum information, quantum communication, quantum metrology, and quantum computation.[2–9] The central point of convergence of all these quantum technologies is to enhance information security by establishing a global-scale network of quantum internet[4,10] interconnected through different nodes and channels at various locations of the earth while accessing the advantage of quantum communication. Quantum communication, such as quantum key distribution (QKD),[5,7,11] is considered superior to its classical counterpart due to the encryption of the information through the use of the resourcefulness of photonic entanglement. Core to QKD is the need for an entangled photon source (EPS)[12–15] with high state fidelity, while long-distance QKD networks through optical fiber or free-space channels demand high brightness EPSs. One of the straightforward approaches to achieve this is to enhance the brightness of the EPS based on spontaneous parametric down-conversion (SPDC) in $\chi^{(2)}$ nonlinear optical crystals.[9,12–14,16,17] Efforts in this regard include replacing critically phase-matched crystals[12,13,15] with quasi-phase-matched periodically poled crystals,[9,18] including potassium titanyl phosphate (PPKTP) crystals in a type-II phase-matching geometry,[19–21] as well as in a type-0 phase-matching geometry.[22] Among all the nonlinear crystals, PPKTP crystals in type-II phase-matching geometry have been used widely for entangled photon sources[21] despite exploring the full benefits of long interaction length and the high nonlinear coefficient as achieved in type-0 phase-matching geometry. This is due to the practical limitations in separating and detecting collinear, co-polarized paired photons of the same wavelength individually. Unfortunately, in such crystals the refractive index is strongly dependent[23–25] on temperature, the wavelength of the interacting radiation, and the angle of the optic axis, so that the key SPDC features such as cone angle and the ring radius of the SPDC photons changes with any of these physical parameters. As a result, typical laboratory based SPDC experiments have careful selection of the laser, stringent stabilization of the pump wavelength to avoid mode hopping and mode jitter, and dynamic control of the crystal temperature (for quasi-phase matched crystals) or precise angle control (for birefringent phase matched crystals). Although these stringent requirements are easily addressable in laboratory conditions, deploying such sources outside the laboratory is hindered by the complexity of the solution, for example, satellite-based applications demands a stringent mass and power budget[26] so a wish-list of solutions is

S. Singh, V. Kumar, A. Ghosh, G. K. Samanta
Photonic Sciences Lab
Physical Research Laboratory
Ahmedabad, Gujarat 380009, India
E-mail: sandeep@prl.res.in

S. Singh
Indian Institute of Technology-Gandhinagar
Ahmedabad, Gujarat 382424, India

A. Forbes
School of Physics
University of the Witwatersrand
Johannesburg 2050, South Africa

The ORCID identification number(s) for the author(s) of this article can be found under https://doi.org/10.1002/qute.202200121

DOI: 10.1002/qute.202200121

not viable. Therefore, it is essential to develop entangled photon sources with relaxed tolerance to such environmental factors.

Here, we report on a hybrid linear and non-linear solution for a stable and bright quantum source with relaxed tolerances in the stabilization of the crystal temperature, mode hopping, and jitter of the pump laser, as well as the angle of the nonlinear crystal. To verify this concept, we have used both PPKTP crystal and BIBO (bismuth borate) crystals producing non-collinear, degenerated down-converted photons through quasi-phase-matching (QPM) and birefringent phase-matching (BPM), respectively, and transformed the annular SPDC ring into what we call a "perfect" ring using an axicon and Fourier transforming lens. We show that while the SPDC output varies tremendously with changing conditions, the hybrid system produces a stable output across a wide variation in external factors. The result is a bright entangled photon source that is tolerance-enhanced, making this approach suitable for deployable quantum sources in non-ideal environments.

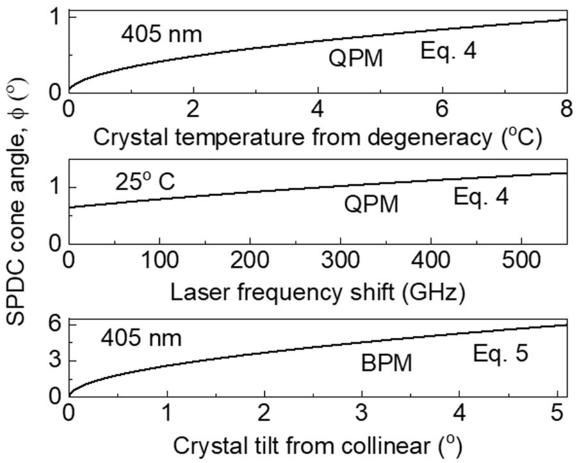

Figure 1. Variation of the SPDC cone angle, ϕ, with the crystal temperature (top panel) and laser frequency shift (middle panel) for the quasi phase matching condition (QPM) given in Equation (4). In the bottom panel the results are shown for the birefringent phase matching (BPM) condition given by Equation (4), here as a function of crystal tilt angle.

2. Theory and Experiment

The intensity distribution of the downconverted photons for a nonlinear crystal of length, L, can be represented as follows,

$$I_{\text{SPDC}} \approx \text{sinc}^2(\Delta k L/2) \tag{1}$$

where the momentum mismatch Δk for the non-collinear, degenerate photons for type-0, first order quasi-phase matching, and type-I birefringent phase matching are respectively given as,

$$\Delta k = k_{\text{p}} - k_{\text{s}}\cos(\phi) - k_{\text{i}}\cos(\phi) - \frac{2\pi}{\Lambda} \tag{2}$$

and

$$\Delta k = k_{\text{p}} - k_{\text{s}}\cos(\phi) - k_{\text{i}}\cos(\phi) \tag{3}$$

Here, $k_{\text{p,s,i}} = \frac{2\pi n_{\text{p,s,i}}}{\lambda_{\text{p,s,i}}}$ is the wavevector and $n_{\text{p,s,i}}$ is the refractive index of the medium for the pump, λ_{p}, signal, λ_{s}, and idler, λ_{i}, wavelengths. Λ is the period of the periodically poled nonlinear crystal and ϕ is the angle the signal and idler wave vectors make with the pump wave vector along the propagation direction. For degenerate ($\lambda_{\text{s}} = \lambda_{\text{s}} = 2\lambda_{\text{p}}$), non-collinear, type-0 ($e \rightarrow e+e$) and type-I ($o \rightarrow e+e$) phase matching, the cone angle, ϕ, of the down-converted photons can be represented using Equations (2) and (3) as

$$\phi_{\text{QPM}} = \arccos\left(\frac{n_{\text{p}}^{e}}{n_{\text{s}}^{e}} - \frac{\lambda_{\text{p}}}{n_{\text{s}}^{e}\Lambda}\right) \tag{4}$$

and

$$\phi_{\text{BPM}} = \arccos\left(\frac{n_{\text{p}}^{o}}{n_{\text{s}}^{e}(\theta)}\right) \tag{5}$$

where QPM and BPM refer to quasi phase matching and birefringent phase matching, respectively. Here, θ is the angle of the optic axis with the propagation direction. We plot the effect of this in **Figure 1** with the help of the dispersion relations of PPKTP[27] and BIBO[28] crystals, clearly showing how the environmental factors influence cone angle and thus the shape and size of the SPDC output. To circumvent this we adopt the approach illustrated in **Figure 2**a. The core idea is to treat the SPDC ring as similar to a hollow Gaussian beam (HGB): a dark core beam with annular intensity distribution and plane wavefront. What happens when such a beam is incident on an axicon? The answer is that it forms a displaced Bessel beam, the displacement determined by the annular ring radius.[29] Interestingly, the Bessel beam itself remains unchanged with ring size as its radial structure is determined by the cone angle of the axicon. On the other hand, it is well known that the Fourier transformation of a Bessel beam results in a perfect annular intensity distribution with a ring radius that depends on the radial wavevector of the Bessel beam.[30,31] Therefore, for a fixed radial distribution of the Bessel beam, the position and size of the "perfect" ring is constant and independent to the change in the input beam to the axicon. To see how this can be exploited in SPDC experiments, consider the present experiment: a pump photon on propagation through the nonlinear crystal (PPKTP or BIBO) splits into pairs of degenerate daughter photons, obeying conservation of momentum and energy. The generated photons are distributed over an annular ring with an intensity distribution given by Equation (1). After collimation by lens L1, the spatial distribution of the photons is transformed into a zero-order Bessel beam of fixed radial wavevector after propagation through the axicon. Given that the Fourier transformation can be possible by putting the object after the lens,[32] the lens L2 of focal length, f, in combination of the axicon placed at a distance $f - D$ behind the lens Fourier transforms the zero-order Bessel beam into a perfect annular ring at the back focal plane of the lens, independent to the change in the spatial distribution of the generated photons. Here, D is the distance of the axicon from the back focal plane of the lens, $L2$. One can then write the intensity distribution of the perfect annular ring as

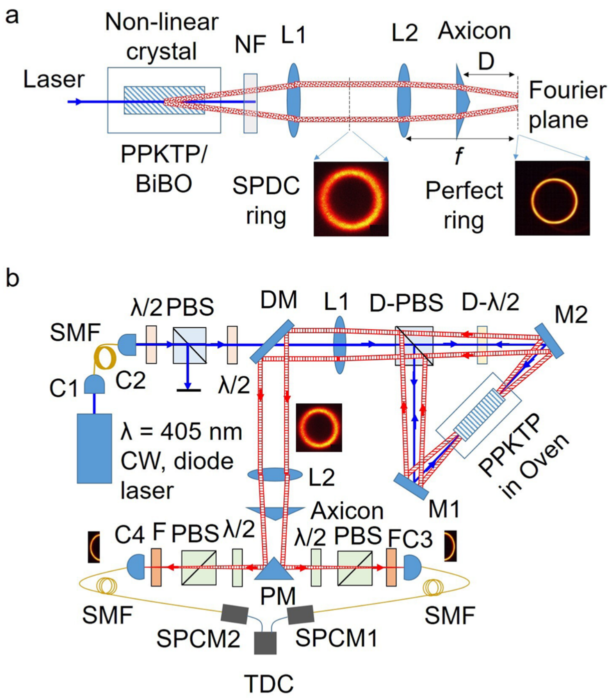

Figure 2. a) Pictorial representation of the basic principle of downconverted photons with "perfect" annular intensity distribution. b) Schematic of the experimental setup. $\lambda/2$: half-wave plates; PBS: polarizing beam splitter cube; DM: dichroic mirror; L1–2: lenses; M1–2: mirrors; PPKTP: periodically poled KTP crystal; F: interference filter; PM: prism mirror, C1-4: fiber couplers, SMF: single-mode fiber, SPCM1-2: single-photon counting modules; TDC: time to digital converter. (Inset) ICCD image of the spatial profile of single photons.

$$I_{\mathrm{Perfect}} = \frac{w_{\mathrm{g}}^2}{w_{\mathrm{D}}^2} \exp\left(-\frac{2(\rho\frac{f}{\mathrm{D}} - \rho_{\mathrm{r}})^2}{w_{\mathrm{D}}^2}\right) \tag{6}$$

where, w_g is the beam waist radius of the Gaussian beam confining the Bessel Gauss beam. The perfect annular ring of width, $2w_D = 1.65\ w_0$, (w_0 is the Gaussian beam waist at the focus), is formed at, $\rho = \frac{D}{f}\rho_r$ with a modified ring radius, $\rho_{\mathrm{r}} = D\sin((n-1)\alpha)$, where n and α are the refractive index and the apex angle of the axicon, respectively. As a result, a perfect annular ring of constant width is formed irrespective of the ring size of the SPDC photons generated by the crystals, making the downconverted photons insensitive to the fluctuations of the phase-matching parameters to external environments.

To validate our approach, we have devised the experiment shown schematically in Figure 2b. A continuous-wave, single-frequency (linewidth ≈12 MHz) laser providing output power of 50 mW at a wavelength of 405 nm was used as a pump source. The mode filtering system comprised of two fiber collimators, C1 and C2, and a single mode fiber, SMF, was used to transform the laser output in a Gaussian beam. A combination of the $\lambda/2$ plate and the polarizing beam splitter (PBS) cube was used to control the pump power in the experiment. A second $\lambda/2$ plate was used to transform the horizontal polarization state of the pump into diagonal to maintain equal pump power of the clock-wise and counter-clockwise beams of the polarization in the Sagnac interferometer, the latter was comprised of a dual-wavelength PBS (D-PBS) and two plane mirrors, M1 and M2. A 20-mm long and 2 × 1 mm^2 PPKTP crystal placed at the center of the Sagnac interferometer between mirrors, M1 and M2, and was pumped from both sides using the plano-convex lens (L1) of focal length, f = 150 mm. The PPKTP crystal had a single grating period, Λ = 3.425 µm, and was housed in an oven with temperature stability of ±0.1 °C to produce degenerate down-converted photons at a wavelength of 810 nm owing to type-0 ($e \rightarrow e$+e), non-collinear, phase matching of the pump photons. The dual-wavelength $\lambda/2$ plate ($D-\lambda/2$), at both 405 and 810 nm, transformed the polarization of both pump and the down-converted photons from horizontal to vertical and vice versa. The counter-propagating SPDC photons of the polarization Sagnac interferometer on recombination by the D-PBS resulted in a Bell state.[9] After collimation by the lens, L1, and subsequent extraction by the dichroic mirror, DM, the down-converted photons in the annular intensity profile (see inset image) were transformed into an annular ring of fixed diameter using a combination of lens and axicon. The Fourier transform of the Bessel beam generated by the axicon placed after the lens[31,32] was transformed into an annular ring at the back focal plane of the lens L2, of focal length, f =100 mm. The apex angle of the axicon was 178.4 °C. The annular intensity profile of the down-converted photons was divided into two symmetric half rings (see the inset images) using the prism mirror, PM (gold-coated right-angle prism). The pair photons were collected by the fiber couplers, C3 and C4, placed at the focal plane of the lens, L2. The polarization states of the photons were studied using the combination of $\lambda/2$ plate and PBS. The interference filter, F, of spectral width 3.2 nm centered at 810 nm, was used to extract down-converted photons from the background. The single-photon counting modules, SPCM1-2, connected to the fiber couplers, C3 and C4, using single mode fiber (SMF) or multimode fibers, and the time-to-digital converter (TDC) were used to measure the single counts and coincidence counts. The temporal coincidence window for all the measurements was 1.6 ns.

The size of the annular intensity profile and corresponding photon density depends on the position of the axicon from the Fourier plane. However, placing the axicon close to the Fourier plane to increase the overall photon counts adds mechanical constraints to the detection and analyzer systems. In such a case, a 4-f imaging system (not shown here) is used to collect and analyze the down-converted photons. Note that this approach also works with type-0 phase-matching by sandwiching two type-0 crystals with orthogonal poling period direction in dual-crystal scheme.

3. Results

To verify the concept of the SPDC perfect ring, we have measured the spatial distribution of the down-converted photons before the lens, L2, and at it's Fourier plane while varying the pump wavelength, crystal angle, and crystal temperature. The results are shown in **Figure 3**. For this study, we have used the polarization state of the input laser to be either horizontal for BiBO crystal or vertical for PPKTP crystal. As evident from the first column, Figure 3a–c, the spatial distribution of the SDPC photons generated by the PPKTP crystal at a temperature of 25 °C changes from the collinear Gaussian distribution to the non-collinear annular

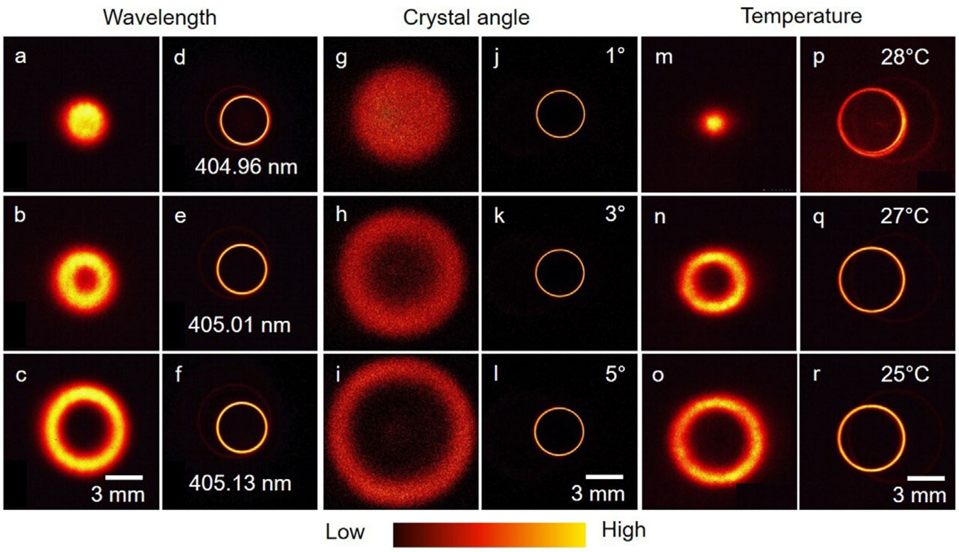

Figure 3. Variation of the spatial distribution of the a–c) SPDC ring and d–f) "perfect" ring as a function of pump wavelength for a fixed temperature of 25 °C of PPKTP crystal. Dependence of the spatial distribution of the g–i) SPDC ring and j–l) "perfect" ring as a function of phase matching angle of BIBO crystal for a fixed pump wavelength of 405.01 nm. Variation of the spatial distribution of the m–o) SPDC ring and p–r) "perfect" ring as a function of PPKTP crystal temperature for a fixed pump wavelength of 405.01 nm.

ring for pump wavelengths 408.96, 405.01, and 405.13 nm. However, the diameter of the "perfect" ring as shown in the second column, Figure 3d–f, recorded at the Fourier plane is the same for all pump wavelengths and independent of the spatial distribution of the SPDC photons. Similarly pumping the BIBO crystal having cut angle, $\theta = 151.7°$ ($\phi = 90°$) in optical yz-plane for perfect phase-matching of non-collinear type-I ($o \rightarrow e{+}e$) degenerate down-converted photons at 810 nm, with the laser wavelength λ_p = 405.01 nm, we have varied the crystal angle and recorded the intensity distribution of the SPDC ring and the "perfect" ring as shown in Figure 3g–i, and Figure 3j–l, respectively. As expected the spatial distribution of the SPDC photons changes from the collinear geometry to non-collinear geometry with increasing diameter of the annular ring for the crystal tilt angle 1°, 3°, and 5° whereas the diameter of the "perfect" ring is constant for all crystal angles. On the other hand, to verify the "perfect" ring for the variation of crystal temperature, we pumped the PPKTP crystal with the laser wavelength of λ_p= 405.01 nm, and recorded the intensity profile of the SPDC ring and the "perfect" ring for crystal temperature 28, 27, and 25 °C. As evident from Figure 3m–o, the spatial distribution of the SPDC photons changes from the collinear geometry at 28 °C to the non-collinear annular ring of increasing diameter with the crystal temperature 27 and 25 °C. However, the diameter of the "perfect" ring as, shown in Figure 3p–r irrespective of the change in the spatial profile of the SPDC photons due to the change in the phase-matching condition. The current results reveal that the position and size of the "perfect" ring of the down-converted photons are insensitive to the physical parameters influencing the phase-matching condition. As a result, the photon collection optics set to couple the pair photons on the diametrically opposite side of the annular ring does not see any effect of the change in the physical parameters responsible for the phase-matching of the nonlinear crystal. Therefore, the present technique enables the use of relaxed phase-matching parameters for the practical implementation of the down-converted photon-based quantum sources.

To gain further insight, we have recorded the spatial profile of the SPDC ring and the "perfect" ring with the increase of crystal temperature from 21 °C with a step of 0.5 °C for the PPKTP crystal and the tilt of BIBO crystal and measured the diameter and the width of the rings with results shown in **Figure 4**. As evident from Figure 4a, the radius of the SPDC ring (black squares) increases with the PPKTP crystal temperature, $\Delta T = T_o - T$, away from the degenerate collinear phase-matching temperature, T_o = 28 °C. However, the radius of the "perfect" SPDC ring (red circles) remains constant at ≈2.73 mm. The variation in the cone angle or the diameter of the annular ring of the SPDC photons with temperature is the same as that of the previous report[9] and closely matches the theoretical fit (black line) based on Equation (4) and the dispersion relation of ref. [27]. However, the shift in the temperature of the degenerate collinear SPDC photons from 36 °C as shown in the report[9] to 28 °C can be attributed to the change in the laser wavelength. On the other hand, the width (FWHM) of the SPDC ring (open squares), as shown in Figure 4a, remains constant for all phase matching temperatures, but the width of the "perfect" SPDC ring (open circles) is constant (≈200 µm) with temperature (up to 3 °C) and increases to 380 µm at 7 °C. In literature, it is observed that the width of the perfect vortex increases with the order of the input vortex.[33] Therefore, to get a better perspective on the variation of the width of the SPDC perfect ring, we have calculated the vortex ring radius with the order using Equation (3) of ref. [34] and fit (blue line) to the experimental results (black square) in Figure 4a. As evident from Figure 4a, the rate of increase of the SPDC ring radius with temperature is faster than that of the vortex ring radius with its order. The change in the SPDC ring radius for the crystal temperature 7 °C away from the collinear phase-matching temperature (28 °C) is equivalent to the change in the ring radius of the vortex beam

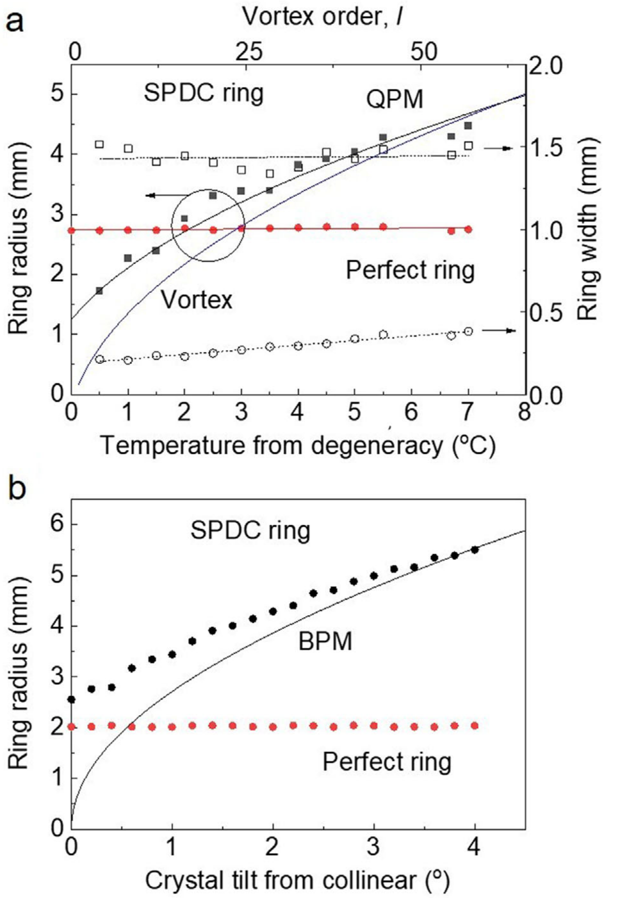

Figure 4. a) Variation of the radius of the SPDC ring (black dots), and the SPDC perfect ring (red dots) with the PPKTP crystal temperature away from degeneracy at T_o=28 °C. The black line is the theoretical fit of Equation (4) to the experimental results and the blue line represents the variation of vortex beam radius with its order. Variation of the width of the SPDC ring (open square) and "perfect" ring (open circle) with the crystal temperature. Lines are guide to eyes. b) Variation of the radius of the SPDC ring (black dots) and the SPDC perfect ring (red dots) with the tilt in the phase-matching angle of the BIBO crystal away from degenerate collinear phase-matching angle, $\theta_o = 152°$. The black line is the theoretical fit of Equation (5) to the experimental results.

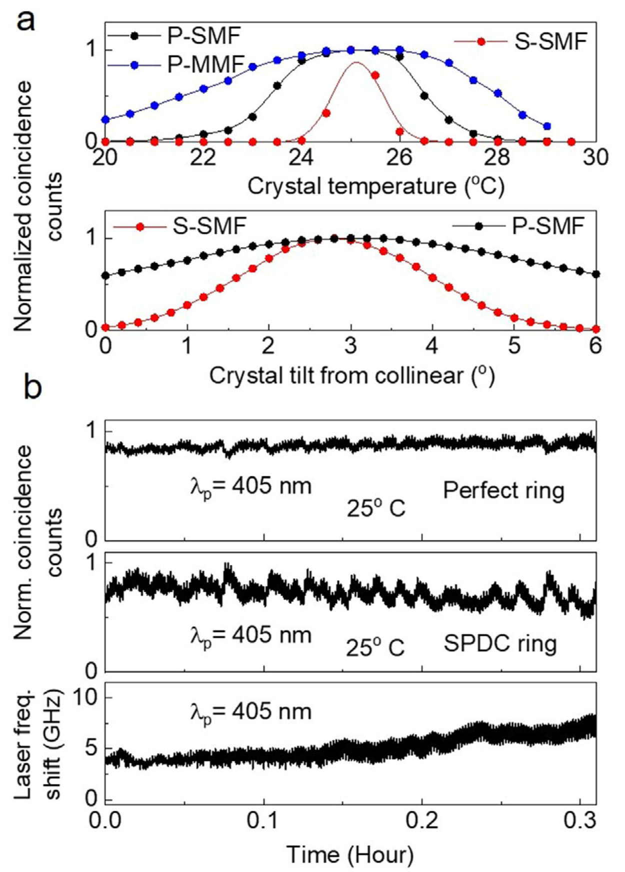

Figure 5. a) Variation of coincidence counts of the paired photons collected from the diametrically opposite points of the SPDC ring and "perfect" ring with PPKTP crystal temperature and the tilt angle of the BIBO crystal. b) Stability of the coincidence counts of the quantum source based on the "perfect" ring and SPDC ring with the variation of laser frequency over 15 min.

for an order increase of 50. Therefore, using the similar analogy of ref. [33], we can confirm that the increase in the width of the SPDC perfect ring (open circles of Figure 4a) is due to the increase in the SPDC ring radius with crystal temperature. One can use the similar treatment of ref. [33] to reduce the width of the SPDC perfect ring by increasing the radius of the "perfect" ring by simply moving the axicon close to the lens L2. However, such a proposition will reduce the photon number density collected by the fibers and the overall brightness of the paired photon source. Similarly, as evident from Figure 4b, the radius of the SPDC ring (black dots) increases with the tilt angle of BIBO crystal, $\Delta\theta = \theta_o - \theta$, away from the degenerate collinear phase-matching angle, $\theta_o = 152°$. However, the radius of the "perfect" SPDC ring (red dots) remains constant at ≈2 mm. The variation in the cone angle or the diameter of the annular ring of the SPDC photons with tilt closely matches the theoretical fit (black line) based on Equation (5) and the dispersion relation of ref. [28]. On the other hand, due to the unavailability of suitable laser diodes with controlled wavelength variation in the lab, we could not test the current scheme for more wavelengths. However, it is evident from the first and second columns of Figure 3, that the radius of the SPDC perfect ring is constant despite the variation of the SPDC ring radius due to the change in the pump wavelength by ±150 GHz making the quantum source insensitive to the mode hop and wavelength jitter of the pump laser.

Proving the generation of the "perfect" SPDC ring insensitive to the external physical parameters influencing the phase-matching process of the nonlinear medium, we have studied the coincidence counts of the photons collected from diametrically two opposite points on the SPDC ring and the "perfect" ring. The results are shown in **Figure 5**. Keeping the laser wavelength and the crystal temperature constant at 405.01 nm and 25 °C, respectively, we have measured the coincidence counts while varying the crystal temperature with the results shown in the first panel of Figure 5a. As evident from Figure 5a, the coincidence counts (red dots) between the pair photons collected using the single-mode fiber from the SPDC ring optimized for a crystal temperature (say, 25 °C) decreases for the crystal temperature away from 25 °C with a temperature bandwidth (FWHM) of 1 °C. However, the coincidence counts for the photons collected using single-mode (black dots) and multimode (blue dots) from the SPDC perfect ring have a temperature bandwidth of 3.2 and 6.5 °C, resulting in a 3.2 and 6.5 times enhancement in the temperature bandwidth. Further analysis reveals that a 10% peak-to-peak fluctuation in the coincidence counts requires the crystal temperature stabilization within ±0.15 °C for the SPDC ring. However, the use of the "perfect" SPDC ring relaxes the temperature stability requirement of ±0.8 and ±1.25 °C for photon collection using single-mode and multimode fibers, respectively. Similarly, pumping the BIBO crystal with a laser wavelength of 405.01 nm, we have measured the coincidence counts for the SPDC ring and the "perfect" ring while varying the tilt of the BIBO crystal away from degenerate collinear phase-matching angle, $\theta_o = 152°$ with the results shown in the second panel of Figure 5a. As evident from Figure 5a, the coincidence counts (black dots) between the pair photons collected using the single-mode fiber from the SPDC ring optimized for a cone angle of 3° vary with the crystal tilt resulting in an angular bandwidth (FWHM) of ≈ 2.5°. However, under the same experimental condition, the angular bandwidth (FWHM) for the "perfect" ring is ≈ 6°, more than two times broader than the SPDC ring. Further analysis reveals that a 10% peak-to-peak fluctuation in the coincidence counts requires the crystal angle stabilization within ±22 mrad for the "perfect" ring, almost three times relaxation as compared to the SPDC ring (angle stabilization within ±8 mrad). Using the PPKTP crystal, we have also measured the stability of the coincidence counts of the "perfect" ring, SPDC ring over 15 min with the wavelength jittering of the laser diode with the results shown in Figure 5b. In doing so, we switched off the temperature stabilization of the laser diode and measured the wavelength using the high-resolution wavemeter (HighFinnese). As evident from Figure 5b, the laser diode has a frequency shift of 6 GHz in 15 min. The simultaneous measurement of the coincidence counts reveals that the quantum source based on the "perfect" ring has a counts fluctuation (standard deviation) of 4.8%, 2.5 times better stable than that of the SPDC ring (standard deviation ≈12.6%) for the pump frequency shift of 6 GHz over 15 min. Due to the unavailability of a suitable laser diode with the controlled variation of frequency, we could not characterize the current technique for higher frequency shift. However, using the dispersion relations[27] of PPKTP crystal and the temperature acceptance bandwidth we can estimate the stable performance of the "perfect" ring-based quantum source for the laser frequency shift of ≈100 GHz.

Confirming the performance of the SPDC source of new architecture requiring relaxed constraints in the physical parameters influencing the phase-matching condition, we have designed the polarization-entangled photon source and characterized it using the standard coincidence measurement technique. Keeping the polarization of the pump laser diagonal, we have rotated the polarization state of one of the pair photons using the analyzer and measured the coincidence with its partner photon collected from the diametrically opposite point of the SPDC perfect ring at a fixed polarization state, H (horizontal), D (diagonal), V (vertical), and A (anti-diagonal). The results are shown in **Figure 6**a. As evident from Figure 6a, we observe a typical quantum interference of the polarized entangled photons for H (black dots), V (blue dots), D (red dots), and A (green dots) projections at the crystal temperature of 25 °C. The solid lines are the best fit for the experimental data. The number of detected entangled paired photons have maximum and minimum values of $\approx 2.2 \times 10^4$ and 7×10^2 Hz mW^{-1} for all polarization projections. The raw fringe visibility for polarization correlation is 94.2 ± 0.06% in H/V bases and 93.8 ± 0.06% in D/A bases confirming the non-local behavior of quantum entanglement. We also have calculated the Bell's parameter to be $S = 2.64 \pm 0.03$, corresponding to a violation of 21 standard deviations, confirming the generation of high-quality entangled photons. Further, we have measured the quantum interference visibility and the coupling efficiency (ratio of the coincidence counts to the square root of the product of the singles counts of two detectors) of the source at different crystal temperatures with the results shown in Figure 6b. As evident from Figure 6b, the interference visibility and the coupling efficiency are constant at ≈93% and 7%, respectively, for almost the entire temperature range; however, the coupling efficiency decreases with crystal temperature toward the collinear phase-matching. Since we are using the highest figure-of-merit of the nonlinear process to generate entangled photons, the growing demands of multiple

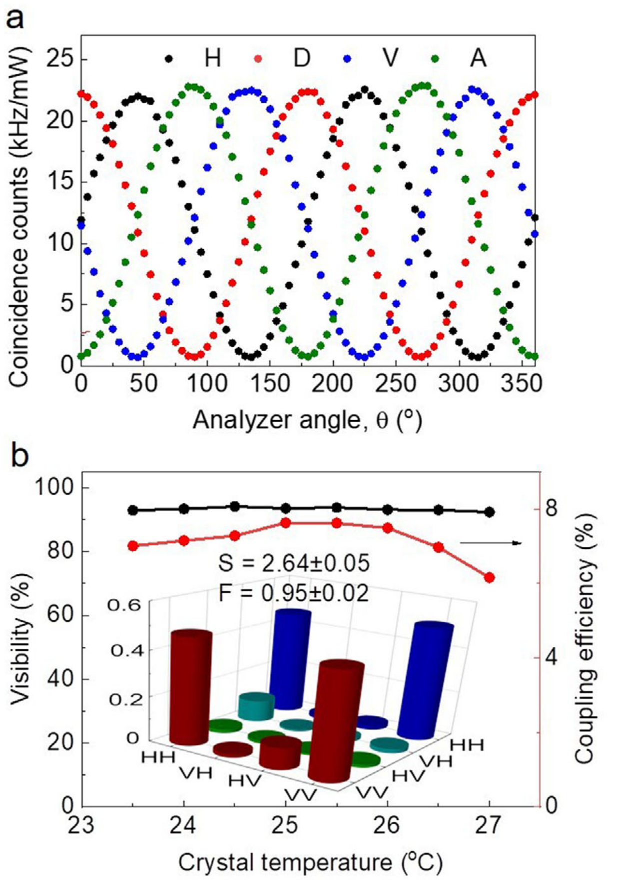

Figure 6. a) Quantum interference of the entangled photons projected at different polarization states, H, D, V, and A. b) Variation of quantum interference visibility (black dots) and coupling efficiency (red dots) with crystal temperature. (Inset) Graphical representation of the absolute values of the density matrix of the entangled photon states. Lines are the guide to the eyes.

Table 1. Qualitative comparison of entanglement properties and the tolerance parameters of entangled photon sources.

	Phase-matching	Nonlinear crystals	Entanglement properties		Tolerance to external parameters		
			Spectral brightness	Fidelity	Temperature	Crystal angle	Pump wavelength
Other studies	BPM	BBO/BIBO[40,41]	Low	High	–	Low	Low
	QPM	PPLN[21,22,42–44]	Moderate	High	High	–	Low
		PPKTP[9,19,45]	High	High	Low	–	Moderate
Current study	BPM	BIBO	Low	High	–	High	High
	QPM	PPKTP	High	High	High	–	High

entangled pairs desirable for advanced quantum optics and information experiments can only be addressed by increasing the coupling/collection efficiency. It is evident from the literature[35–37] that the coupling efficiency depends on the size of fibers effectively imaged onto the crystal plane and the crystal length, scaled to the pump beam waist into the crystal. Therefore, by optimizing these parameters, one can increase the overall entangled photon pair rate of the EPS. Such a study in itself is an interesting topic but beyond the scope of the current work as we have mostly focused on the tolerance of the EPS performance to external perturbations. Again, it is worth noting that the current system architecture results in entangled pair counts of > 0.3 MHz mW^{-1} without considering the losses in the experiment and the efficiency of the detectors. Since the quality of the generated quantum state does not depend on the collection efficiency, we have measured the degree of entanglement of the photon states using the linear tomographic technique.[38] The results are shown in the inset of Figure 6b. From the graphical representation of the absolute values of the density matrix of the generated states (see inset of Figure 6b), we determine the state to be, $|\psi>= \frac{1}{\sqrt{2}}(|HH>-|VV>)$, with a state fidelity of 0.95. As explained previously,[9] we can transform the generated state to another Bell's state by adjusting the position of the crystal[39] in the Sagnac interferometer.

4. Discussion

The approach we have outlined has the benefit of improving the tolerance of EPSs without sacrificing brightness performance, the only approach to allow both to be optimized simultaneously. To see this, consider the comparative analysis of our approach versus other standard approaches based on bulk nonlinear crystals given in **Table 1**. We see that EPSs based on BPM nonlinear crystals such as bismuth borate (BBO) and BIBO can produce entangled state with high fidelity (>0.95) but have exceptionally lower spectral brightness (≈2 kHz mW^{-1}) due to their intrinsic lower nonlinear coefficient ($d_{\text{eff}} \approx 2.2 - 3.4$ pm V^{-1}) and small effective interaction length avoiding spatial walk-off effect,[40,41] severely restricting their usefulness for practical applications. Again, the strong dependence of refractive index on the orientation of the optics axis of such crystal and the wavelength of the interacting radiations demands a tight control in the crystal angle and pump wavelength for stable operation of the EPS. Naturally, efforts have been made to explore QPM based nonlinear crystals with higher nonlinear coefficient including periodically pole lithium niobate (PPLN) and PPKTP to improve the spectral brightness of the EPS. However, due to the practical limitation of fabricating small poling period, the PPLN crystals are used for EPSs in the telecommunication wavelength range,[21,22,42–44] where the single photon detectors are either bulky or inefficient. Exploiting the dispersion relations of PPLN crystal in type-II phase-matching, efforts have been made to improve the tolerance in the crystal temperature,[21] however, such efforts are very wavelength selective and not possible to achieve for EPSs of other wavelengths.

On the other hand, to access the benefits of the compact Si-based single photon detectors with a relatively higher quantum efficiency,[46] bright EPSs are developed using PPKTP crystals. While type-II phase-matched PPKTP crystals offer advantages in terms of simpler experimental setup and the use of longer interaction lengths lead to high spectral brightness (>10 kHz mW^{-1}), and quantum state fidelity, however, such sources have low to moderate tolerance to the external perturbations including crystal temperature and pump wavelength variation. Additionally, the sources require pre or post phase compensation between the pair photons to maintain high quantum state fidelity.[19,45] Recently, PPKTP[9] and PPLN[22] crystals in type-0, non-collinear phase-matching configuration have been explored to develop bright EPSs of degenerate photons in simple and compact experimental configuration without the need for any phase-compensation. While these sources have very high spectral brightness due to the use of the highest figure-of-merit of the nonlinear crystal and state fidelity,[9,22] they have low to moderate tolerance to the perturbation of external parameters including crystal temperature and pump wavelength due to the change in the spatial distribution to the SPDC photons with respect to the fixed photon detection systems. Contrary to all the previous reports on EPSs, the current system architecture enhances the tolerance of the EPS to external perturbations in terms of phase-matching angle, temperature, and pump wavelength while maintaining high spectral brightness and quantum state fidelity. As evident from Table 1, while prior approaches each tick some of the boxes, our approach ticks all the salient boxes.

5. Conclusion

In conclusion, we have demonstrated a novel SPDC configuration where a hybrid solution that incorporates a lens-axicon pair, commonly available in an optics laboratory, was shown to have transformed the conventional SPDC annular ring into a new ring that is insensitive to perturbations, including the variation of the crystal temperature and laser wavelength. The generic experimental scheme, useful for the development of entangled photons at any desired wavelength and time scale, relaxes the stringent temperature stabilization of the crystal by five times and mode hopping and wavelength jitter by 100 GHz. Such demonstration opens up a new approach to robust SPDC sources for reliable deployment in field demonstration of quantum optics experiments.

Conflict of Interest

The authors declare no conflict of interest.

Data Availability Statement

The data that support the findings of this study are available from the corresponding author upon reasonable request.

Keywords

parametric processes, photon polarization, photonic entanglement, quantum key distribution, quantum optics, Sagnac interferometry, structured optical beams

Received: September 20, 2022
Revised: December 8, 2022
Published online: December 30, 2022

[1] G. Weihs, T. Jennewein, C. Simon, H. Weinfurter, A. Zeilinger, *Phys. Rev. Lett.* **1998**, *81*, 5039.
[2] N. Gisin, G. Ribordy, W. Tittel, H. Zbinden, *Rev. Mod. Phys.* **2002**, *74*, 145.
[3] J. L. O'brien, *Science* **2007**, *318*, 1567.
[4] H.-J. Briegel, W. Dür, J. I. Cirac, P. Zoller, *Phys. Rev. Lett.* **1998**, *81*, 5932.
[5] G. Ribordy, J. Brendel, J.-D. Gautier, N. Gisin, H. Zbinden, *Phys. Rev. A* **2000**, *63*, 012309.
[6] A. Sergienko, G. Jaeger, *Contemp. Phys.* **2003**, *44*, 341.
[7] D. Bouwmeester, J.-W. Pan, K. Mattle, M. Eibl, H. Weinfurter, A. Zeilinger, *Nature* **1997**, *390*, 575.
[8] X. Chen, Z. Fu, Q. Gong, J. Wang, *Adv. Photonics* **2021**, *3*, 064002.
[9] M. V. Jabir, G. K. Samanta, *Sci. Rep.* **2017**, *7*, 12613.
[10] H. J. Kimble, *Nature* **2008**, *453*, 1023.
[11] Y. Juan, L. Yu-Huai, L. Sheng-Kai, Y. Meng, C. Yuan, Z. Liang, R. Ji-Gang, C. Wen-Qi, L. Wei-Yue, L. Shuang-Lin, S. Rong, H. Y. Mei, D. Lei, L. Li, Z. Qiang, L. Nai-Le, C. Yu-Ao, L. Chao-Yang, W. Xiang-Bin, X. Feihu, W. Jian-Yu, P. Cheng-Zhi, A. K. Ekert, P. Jian-Wei, *Nature* **2020**, *582*, 501.
[12] P. G. Kwiat, K. Mattle, H. Weinfurter, A. Zeilinger, A. V. Sergienko, Y. Shih, *Phys. Rev. Lett.* **1995**, *75*, 4337.
[13] P. G. Kwiat, E. Waks, A. G. White, I. Appelbaum, P. H. Eberhard, *Phys. Rev. A* **1999**, *60*, R773.
[14] M. Fiorentino, S. M. Spillane, R. G. Beausoleil, T. D. Roberts, P. Battle, M. W. Munro, *Opt. Express* **2007**, *15*, 7479.
[15] M. V. Jabir, M. Apurv Chaitanya, N. Mathew, G. K. Samanta, *Sci. Rep.* **2017**, *7*, 7331.
[16] D. C. Burnham, D. L. Weinberg, *Phys. Rev. Lett.* **1970**, *25*, 84.
[17] W. Louisell, A. Yariv, A. Siegman, *Phys. Rev.* **1961**, *124*, 1646.
[18] P. S. Kuo, V. B. Verma, S. W. Nam, *OSA Continuum* **2020**, *3*, 295.
[19] F. Steinlechner, M. Gilaberte, M. Jofre, T. Scheidl, J. P. Torres, V. Pruneri, R. Ursin, *J. Opt. Soc. Am. B* **2014**, *31*, 2068.
[20] A. Fedrizzi, T. Herbst, A. Poppe, T. Jennewein, A. Zeilinger, *Opt. Express* **2007**, *15*, 15377.
[21] X.-Y. Pan, C. Kurtsiefer, A. Ling, J. A. Grieve, *Appl. Phys. Lett.* **2021**, *119*, 021107.
[22] H. Kim, O. Kwon, H. S. Moon, *Sci. Rep.* **2019**, *9*, 5031.
[23] S. Karan, S. Aarav, H. Bharadhwaj, L. Taneja, A. De, G. Kulkarni, N. Meher, A. K. Jha, *J. Opt.* **2020**, *22*, 083501.
[24] G.-W. Huo, T.-Y. Zhang, R.-G. Wan, M.-Z. Zhang, G. H. Cheng, W. Zhao, in *Photonics and Optoelectronics Meetings (POEM) 2011: Optoelectronic Devices and Integration*, Vol. *8333*, SPIE, Bellingham, WA **2012**, pp. 261–270.
[25] A. Christ, A. Fedrizzi, H. Hübel, T. Jennewein, C. Silberhorn, in *Experimental Methods in the Physical Sciences*, Vol. *45*, Elsevier, Amsterdam, Netherlands **2013**, pp. 351–410.
[26] B. Robert, A. J. Miguel, L. Alexander, *npj Quantum Inf.* **2017**, *3*, 30.
[27] K. Kato, E. Takaoka, *Appl. Opt.* **2002**, *41*, 5040.
[28] H. Hellwig, J. Liebertz, L. Bohatý, *J. Appl. Phys.* **2000**, *88*, 240.
[29] A. S. Rao, G. K. Samanta, *Opt. Lett.* **2018**, *43*, 3029.
[30] P. Vaity, L. Rusch, *Opt. Lett.* **2015**, *40*, 597.
[31] M. V. Jabir, M. Apurv Chaitanya, A. Aadhi, G. K. Samanta, *Sci. Rep.* **2017**, *6*, 21877.
[32] J. Goodman, *Laser Diode Modulation and Noise*, 3rd ed., Roberts and Company Publishers, Greenwood Village, CO **2004**.
[33] J. Pinnell, V. Rodríguez-Fajardo, A. Forbes, *Opt. Lett.* **2019**, *44*, 5614.
[34] S. G. Reddy, C. Permangatt, S. Prabhakar, A. Anwar, J. Banerji, R. P. Singh, *Appl. Opt.* **2015**, *54*, 6690.
[35] F. A. Bovino, P. Varisco, A. Maria Colla, G. Castagnoli, G. Di Giuseppe, A. V. Sergienko, *Opt. Commun.* **2003**, *227*, 343.
[36] A. Anwar, P. Chithrabhanu, S. G. Reddy, N. Lal, R. Singh, *Opt. Commun.* **2017**, *382*, 219.
[37] B. Septriani, J. A. Grieve, K. Durak, A. Ling, *Optica* **2016**, *3*, 347.
[38] D. F. V. James, P. G. Kwiat, W. J. Munro, A. G. White, *Phys. Rev. A* **2001**, *64*, 052312.
[39] A. Predojević, S. Grabher, G. Weihs, *Opt. Express* **2012**, *20*, 25022.
[40] A. Sansa Perna, E. Ortega, M. Gräfe, F. Steinlechner, *Appl. Phys. Lett.* **2022**, *120*, 074001.
[41] A. Halevy, E. Megidish, L. Dovrat, H. Eisenberg, P. Becker, L. Bohatỳ, *Opt. Express* **2011**, *19*, 20420.
[42] S. Arahira, T. Kishimoto, H. Murai, *Opt. Express* **2012**, *20*, 9862.
[43] W. Ueno, F. Kaneda, H. Suzuki, S. Nagano, A. Syouji, R. Shimizu, K. Suizu, K. Edamatsu, *Opt. Express* **2012**, *20*, 5508.
[44] P. S. Kuo, T. Gerrits, V. Verma, S. W. Nam, O. Slattery, L. Ma, X. Tang, in *Advances in Photonics of Quantum Computing, Memory, and Communication IX*, vol. *9762*, SPIE, Bellingham, WA **2016**, pp. 108–116.
[45] S. M. Lee, H. Kim, M. Cha, H. S. Moon, *Opt. Express* **2016**, *24*, 2941.
[46] M. D. Eisaman, J. Fan, A. Migdall, S. V. Polyakov, *Rev. Sci. Instrum.* **2011**, *82*, 071101.